Terahertz band-stop filter based on graphene cavity

Zhao Ze-Jiang, Li Jiu-Sheng ✉

Centre for THz Research, China Jiliang University, Hangzhou 310018, People's Republic of China
✉ *E-mail: forever-li@126.com*

Published in Micro & Nano Letters; Received on 16th June 2017; Revised on 22nd October 2017; Accepted on 23rd November 2017

In order to obtain ultra-compact and ultra-narrow bandstop performances, the work presents a terahertz filter based on graphene cavities, which consists of four graphene cavities and a graphene waveguide on SiO_2/Si substrate. To demonstrate the feasibility of the approach, numerical simulation performed with the aid of the finite-element method is used to evaluate the terahertz performance of the proposed device. The structure rejects the signals at the frequencies from 5.9978 to 6.002 THz with >20 dB suppression. The high-Q band-rejection terahertz wave filter with four graphene cavities provides of 1500. The dimensions of the presented terahertz wave band-stop filter are of 22.5 μm × 18.0 μm. The high-performance, compact-size, and low-cost filter is designed for reducing the interference in future terahertz systems.

1. Introduction: Recently, with the rapid development of terahertz wave sources [1–3] and detectors [4], there is a high demand for terahertz components such as splitters, absorbers, waveguides, filters, polarisers, modulators, and switches [5–9]. One of the most important devices in terahertz applications is terahertz wave filter. Up to now, several various structure designs of terahertz filters have been reported [10–12]. Some theoretical and experimental research on these terahertz wave filters have been done using traditional material such as metallic hole arrays [13], photonic crystals [14], matematerials [15–17] or frequency-selective surfaces [18]. Often these structures are not compatible with planar integrated terahertz circuits. Additionally, many of these filters are difficult to fabricate and require significant machining or other specialised processes to fabricate. This has limited the practical use of these filters. Recently, due to the special properties, graphene has been considered for various electronic and communication applications. Also, surface plasmon polarisation waves in graphene and their dependency on electrical conductivity and chemical potential have been demonstrated [19]. In 2016, Danaeifar *et al.* [20] proposed a graphene-based tunable terahertz bandpass filter. The effects of temperature and mechanical deformations on the graphene nanodiodes and nanotransistors properties have been studied by Sadeghzadeh *et al.* [21–23]. However, with rapid development and diversified applications of terahertz technology, the development of terahertz filter is still lagging behind. The high-performance, compact-size, and low-cost terahertz filters are commonly required.

In this Letter, we introduce the principle and demonstrate the feasibility of a tunable graphene-based cavities band-stop filter for terahertz region applications. The band-stop centre frequency of the graphene-based terahertz filter can be tunable by changing the applied electric field without change the configuration. The finite-element method (FEM) is performed to investigate the transmission properties of the proposed device. Our results show that the 3 dB bandwidth of our proposed band-stop filter is from 5.998 to 6.002 THz and the largest stop-band attenuation is of −27 dB. The dimensions of the presented terahertz wave filter are of 22.5 μm × 18.0 μm. With the help of the graphene cavities, the total size of the terahertz filter is reduced dramatically when comparing with the traditional material. It anticipated that our proposed compact device is potentially interesting for the terahertz wave integrated circuit technology.

2. Theory analysis: Fig. 1 shows a terahertz wave filter by using graphene cavity on SiO_2/Si substrate. In this Letter, the graphene is treated as an ultra-thin film with a thickness of 0.34 nm. The detailed two-dimensional topology of the proposed terahertz wave filter is depicted in Fig. 2. The graphene dielectric cavities possess mirror symmetry with respect to the reference planes. Note that the g denotes the gap between the rectangular graphene waveguide and four graphene cavities, L is the side length of the square graphene cavities and d is the distance between two parallel graphene cavities.

For the multi-cavity-coupled waveguide systems, the dynamic transmission features can be investigated by a temporal coupled-mode theory [24, 25]. Here, to simplify the theoretical model, the terahertz wave propagation and coupling losses are not considered. For the harmonic time dependence of $e^{-j\omega t}$, the temporal normalised mode amplitudes a_i of the ith cavity ($i = 1, 2, 3, 4$) can be described as [26, 27]

$$\frac{da_i}{dt} = (-j\omega_i - \kappa_{o,i} - \kappa_{e,i})a_i + e^{j\theta_i}\sqrt{\kappa_{e,i}}S^{(i)}_{+,\text{in}} + e^{j\theta_i}\sqrt{\kappa_{e,i}}S^{(i)}_{-,\text{in}} \quad (1)$$

where ω_i represents the resonance frequency of the ith cavity, $\kappa_{o,i}$ is the decay rate of the field due to internal loss in the ith cavity, and $\kappa_{e,i}$ is the decay rate due to the energy escape into the waveguide, θ_i is the phase of coupling coefficient. The decay rates satisfy the relationships $\kappa_{o,i} = \omega_i/(2Q_{o,i})$, $\kappa_{e,i} = \omega_i/(2Q_{e,i})$, $Q_{o,i}$ and $Q_{e,i}$ stand for the intrinsic and coupling quality factors of the ith cavity, respectively. The amplitudes of the incoming and outgoing waves in the straight waveguide are depicted by $S^{(i)}_{p,\text{in}}$ and $S^{(i)}_{p,\text{out}}$ ($i = 1, 2, 3, 4$), respectively. The subscript $p = \pm$ represents two propagating directions of waveguide modes, as shown in Fig. 2. From energy conservation, the outgoing waves of the ith cavity can be defined as

$$S^{(i)}_{-,\text{out}} = S^{(i)}_{-,in} - e^{-j\theta_i}\sqrt{\kappa_{e,i}}a_i \quad (2)$$

$$S^{(i)}_{+,\text{out}} = S^{(i)}_{+,in} - e^{-j\theta_i}\sqrt{\kappa_{e,i}}a_i \quad (3)$$

The propagation terahertz waves in the straight waveguide should satisfy the relationship: $S^{(i)}_{-,\text{in}} = S^{(i+1)}_{-,\text{out}}e^{j\varphi}$ and $S^{(i+1)}_{+,\text{in}} = S^{(i)}_{+,\text{out}}e^{j\varphi}$ ($i = 1, 3$). $\varphi = 2\pi d\text{Re}(n_{\text{eff}})/\lambda_0$ is the phase difference between the two graphene cavities, λ_0 is the wavelength of the incident source, n_{eff} is the effective refractive index of the SPP mode. The dispersion relation of the fundamental SPP mode in the graphene waveguide is given by

$$\tanh\left(\sqrt{n^2_{\text{eff}} - k_0(W+g)/2}\right) = \frac{-\sqrt{n^2_{\text{eff}} - \varepsilon_{\text{graphene}}(\omega)}}{\varepsilon_{\text{graphene}}(\omega)n_{\text{eff}}} \quad (4)$$

doi: 10.1049/mnl.2017.0386

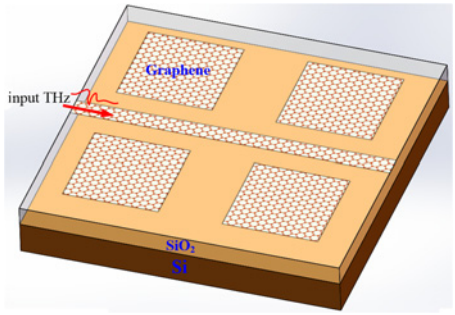

Fig. 1 *Three-dimensional structure of the proposed terahertz filter*

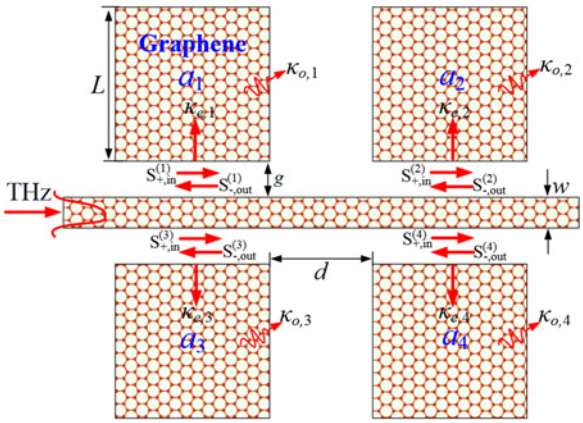

Fig. 2 *Two-dimensional view schematic of the four-cavity-coupled graphene waveguide*

where n_{eff} is the effective refractive index of the SPP wave in the waveguide, $k_0 = 2\pi/\lambda_0$ is the free-space wave vector, g is the gap between the straight waveguide and square graphene cavity, W and ω are the width of the graphene waveguide and the angular frequency of the incident terahertz wave, respectively. In this article, since the field everywhere oscillates as $e^{-j\omega t}$, and $da_i/dt = -j\omega a_i$, the relation between incoming and outgoing waves of the ith cavity can be expressed as

$$S^{(i)}_{-,in} = \frac{\kappa_{e,i}}{j(\omega_i - \omega) + \kappa_{o,i}} S^{(i)}_{+,in} + \frac{j(\omega_i - \omega) + \kappa_{o,i} + \kappa_{e,i}}{j(\omega_i - \omega) + \kappa_{o,i}} S^{(i)}_{-,out} \quad (5)$$

$$S^{(i)}_{+,out} = \frac{j(\omega_i - \omega) + \kappa_{o,i} - \kappa_{e,i}}{j(\omega_i - \omega) + \kappa_{o,i}} S^{(i)}_{+,in} - \frac{\kappa_{e,i}}{j(\omega_i - \omega) + \kappa_{o,i}} S^{(i)}_{-,out} \quad (6)$$

The dip of the transmission spectra of our presented structure with graphene cavities can be given by $\lambda_m = 4n_{\text{eff}}L/(2m+1)$, where $n_{\text{eff}} = \beta/k_0$ (e.g. $n_{\text{eff}} = 16.5$ at 6 THz), L is the side length of the rectangle cavity, the positive integer m is the order of the resonance mode in the graphene cavities. The dip of the transmission spectra of the plasmonic system with graphene cavity coupled to a straight waveguide can be written as $f_m = [(2m+1)c]/(4n_{\text{eff}}L)$, m is the number of cavities. According to theory analysis as above, we can find that the transmission characteristics of the four-cavity-coupled graphene-based terahertz wave filter is related to the gap between the straight waveguide and square graphene cavity (g), the length of the square graphene cavities side length (L), the distance between two square graphene cavities (d), and the effective mode index (n_{eff}) which can be adjusted by the applied bias voltage.

3. Results and discussion: As mentioned above, a commercial available FEM software, COMSOL multiphysics [28, 29], is used to simulate the terahertz wave propagation in the proposed terahertz filter as shown in Fig. 1. The perfectly matched layers are located around the structure as the absorbing boundary condition to evaluate the terahertz wave transmission performance of the presented structure. For simplicity, in the simulation, graphene sheet is free-standing in vacuum with the spatially inhomogeneous conductivity patterns. Fig. 3 shows the transmission spectra for the filter with different geometrical parameter gap (g) between the rectangular graphene waveguide and four graphene cavities, when the other parameters are kept constant to their optimised values. Transmission spectra for widths of 0.4, 0.5, and 0.6 μm are plotted by the black, blue, and red lines, respectively. From Fig. 3, it appears that the gap g mainly controls the bandstop resonance frequency f. One can observe that some transmission dips appear in the spectra, revealing that surface plasmon polaritons in the graphene filter structure are of resonance at 6 THz. From the figure, one can also see that the resonant frequency is of 6.0 THz and the 3 dB bandwidth is 5.998–6.002 THz, when the gap g is of 0.5 μm. Therefore, the gap of the parameter g is set to 0.5 μm.

Fig. 4 illustrates the frequency behaviour of the filter transmission coefficient when the length of the parameter L varies from 5.8 to 7.8 μm when the other parameters are kept constant. From this figure, it appears that the bandstop resonance frequency f moves upward as the length of the parameter L is increased. As it is shown in Fig. 4, when L is equal to 6.8 μm, the resonant frequency is of 6.0 THz while the 3 dB bandwidth is in the frequency

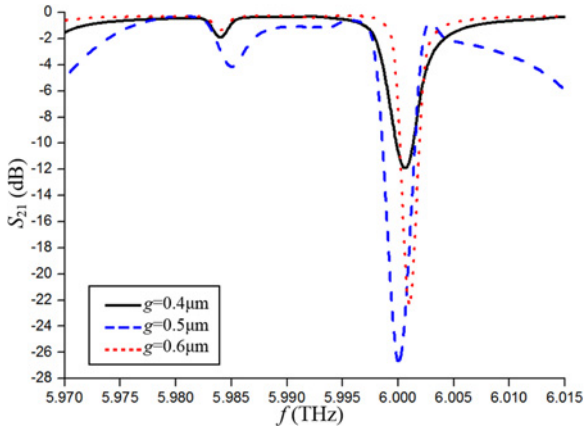

Fig. 3 *Transmission characteristic as a function of different gap (g) between the rectangular graphene waveguide and four graphene cavities*

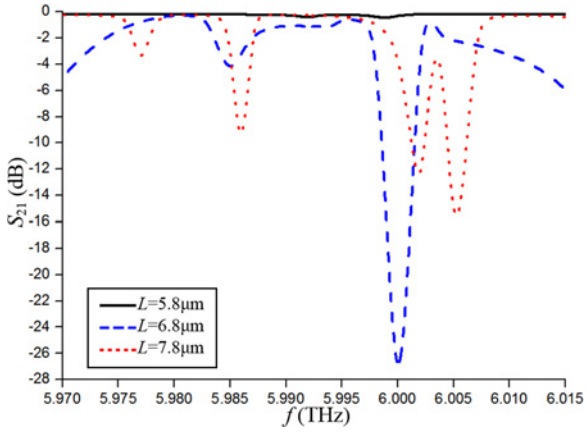

Fig. 4 *Transmission characteristic as a function of different side length L of four square graphene cavities*

range 5.998–6.002 THz. At the same time, the transmission spectrum can also be modified by the change of side length L. Therefore, the length of the parameter L is set to 6.8 μm so to assure a resonance frequency at f.

A different behaviour of the transmission coefficient with respect to the variation of the geometrical parameter d is observed in Fig. 5. In fact, when this parameter d increases from 3.5 to 5.5 μm, while maintaining the other structure parameters to the values of the optimised design, the bandstop resonance frequency moves upwards. In particular, when d is of 4.5 μm, the bandstop resonance frequency and 3 dB bandwidth are 6.0 and 5.998–6.002 THz, respectively. Thus, the parameter d is set to 4.5 μm.

As comparison, the transmission spectra with different width of the waveguide (W) are displayed in Fig. 6. The other parameters are kept as constant. The comparison of the curves in Fig. 6 reveals that the waveguide width has stranger effect on the resonance frequency and bandwidth of the notch filter. The transmission dip with waveguide width tends to exhibit a blue shift. After completing the optimisation process the dimensions of the proposed filter have been set as follows: $L = 6.8$ μm, $g = 0.5$ μm, $d = 4.5$ μm, and $W = 1.4$ μm. A surface plasmon polaritons plane wave source, centred at $f = 6$ THz, is launched at the entrance to the input port and is used to excite graphene surface plasmonic mode in the device. In a two-dimensional structure of graphene by excitation of a TM wave, the surface plasmon polaritons waves can be produced. Fig. 7 shows the steady-state electric field distributions with different cavities charge density obtained by the FEM simulation. Fig. 7*a* shows the electric field distribution of surface plasmon

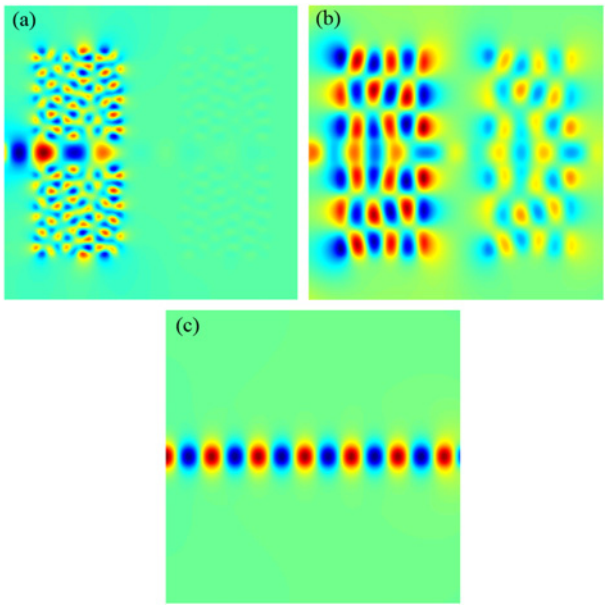

Fig. 7 *Intensity distribution for different chemical potential value in four-graphene-cavity at 6 THz*
a $\mu_c = 0.04$ eV
b $\mu_c = 0.08$ eV
c $\mu_c = 0.12$ eV

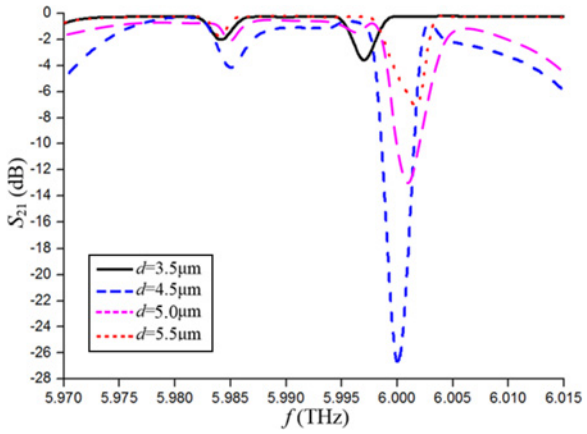

Fig. 5 *Transmission characteristic as a function of different distance d between two parallel graphene cavities*

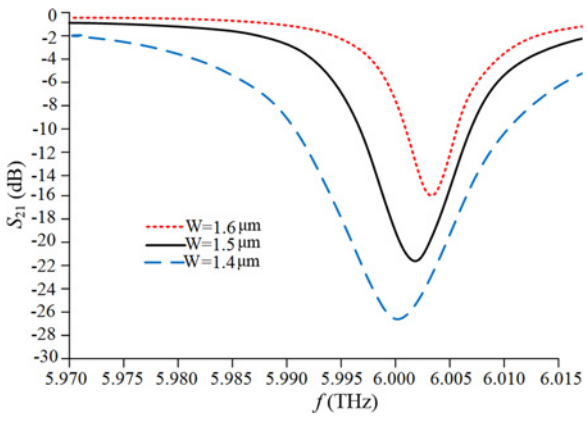

Fig. 6 *Transmission spectra with different width of the waveguide (W)*

polaritons waves in the presented filter at the chemical potential (μ_c) of four square graphene cavities of 0.04 eV. From the figure, one can see that when the resonance condition is satisfied, the incident energy is trapped in the graphene cavities. The input terahertz wave energy is coupled from the graphene waveguide to graphene-based resonant cavities. The electric field distribution clearly shows the coupling process of surface plasmon polaritons between the graphene waveguides and cavities. Note that there is uniform electric field intensity distribution at the two graphene coupling cavities without any back scattering. At this time, the input terahertz wave cannot be transmitted through the graphene-based structure. That is to say, this frequency ($f = 6$ THz) of terahertz wave is notched. Similarly, if a bias voltage (i.e. a chemical potential of $\mu_c^2 = 0.08$ eV) is added on the four square graphene cavities, most of the input terahertz wave energy is coupled into the four graphene cavities and finally a few of the surface plasmonic mode energy can pass through structure, as shown in Fig. 7*b*. Supposing a bias voltage yields a chemical potential of $\mu_c = 0.12$ eV in the graphene cavities, the surface plasmon polaritons from the input graphene cannot be coupled to the graphene-based cavities which is confine in the graphene waveguide without any transmission loss, see Fig. 6*c*. According to Fig. 6, one can see that there would be different electric field intensity in the input and output ports of the present device for different bias voltages. As we know, the conductivity of graphene can be modified by changing chemical potential. Therefore, the coupling process of surface plasmon polaritons between the graphene waveguides and cavities can be controlled by bias voltage.

To illustrate more clearly the performance of the terahertz wave filter, we calculate the transmission spectra of the structure in case of optimised dimensions, as shown in Fig. 8. Fig. 8 shows the transmission spectra for the filter with different chemical potential of four graphene cavities. According to Fig. 7, it can be noted that the terahertz wave transmission is 0.197, 54.126, and 93.025% at $\mu_c = 0.04$ eV, $\mu_c = 0.06$ eV, and $\mu_c = 0.12$ eV operating at 6 THz, respectively. From (1)–(5), we can obtain the stopband centre frequency of the presented filter at 6 THz, which is a good agreement with the simulations.

doi: 10.1049/mnl.2017.0386

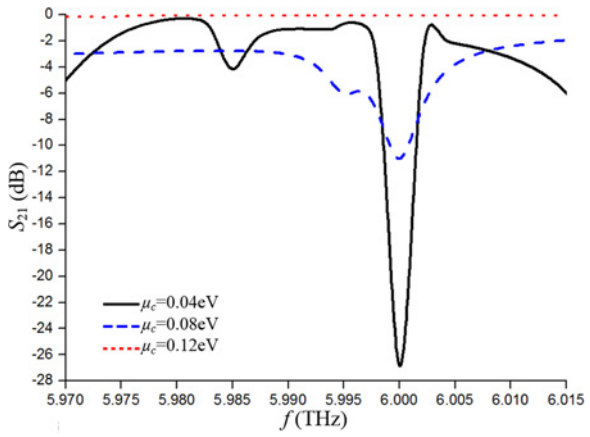

Fig. 8 *Transmission characteristic as a function of different chemical potential of four graphene cavities*

4. Conclusion: To summarise, in this paper we have theoretically demonstrated that four graphene-based cavities bandstop filter is an efficient solution to achieve filter which can be tuned over the terahertz wave frequencies with moderate applied bias voltage changes. The 3 dB bandwidth of the bandstop filter is from 5.998 to 6.002 THz (i.e. bandwidth of 4 GHz) and the largest stop-band attenuation is of −27 dB. Our simulated results are in good agreement with the theoretical predictions. The total size of the present device is only 22.5 μm × 18.0 μm.

5. Acknowledgment: This work was supported by the National Natural Science Foundation of China (grant no. 61379024).

6 References

[1] Adams R., Vijayraghavan K., Wang Q., *ET AL.*: 'GaAs/Al0.15Ga0.85 As terahertz quantum cascade lasers with double phonon resonant depopulation operating up to 172 K', *Appl. Phys. Lett.*, 2010, **97**, p. 131111

[2] Chassagneux Y., Wang Q., Khanna S., *ET AL.*: 'Limiting factors to the temperature performance of THz quantum cascade lasers based on the resonant-phonon depopulation scheme', *IEEE Trans. Terahertz Sci. Technol.*, 2012, **2**, (1), pp. 83–92

[3] Liang G., Liang H., Zhang Y., *ET AL.*: 'Single-mode surface-emitting concentric-circular-grating terahertz quantum cascade lasers', *Appl. Phys. Lett.*, 2013, **102**, p. 031119

[4] Komiyama S., Astafiev O., Antonov V., *ET AL.*: 'A single-photon detector in the far-infrared range', *Nature*, 2000, **403**, pp. 405–407

[5] Wu Y., Ruan X., Chen C., *ET AL.*: 'Graphene/liquid crystal based terahertz phase shifters', *Opt. Express*, 2013, **21**, (18), pp. 21395–21402

[6] Huang Z., Parrott E., Park H., *ET AL.*: 'High extinction ratio and low transmission loss thin-film terahertz polarizer with a tunable bilayer metal wire-grid structure', *Opt. Lett.*, 2014, **39**, pp. 793–796

[7] Pandey S., Kumar G., Nahata A.: 'Slot waveguide-based splitters for broadband terahertz radiation', *Opt. Express*, 2010, **18**, (22), pp. 23466–23471

[8] Pavanello F., Garet F., Kuppam M., *ET AL.*: 'Broadband ultra-low-loss mesh filters on flexible cyclic olefin copolymer films for terahertz applications', *Appl. Phys. Lett.*, 2013, **102**, p. 111114

[9] Mendis R., Nag A., Chen F., *ET AL.*: 'A tunable universal terahertz filter using artificial dielectrics based on parallel-plate waveguides', *Appl. Phys. Lett.*, 2010, **97**, p. 131106

[10] Tao J., Hu B., He X., *ET AL.*: 'Tunable subwavelength terahertz plasmonic stub waveguide filters', *IEEE Trans. Nanotechnol.*, 2013, **12**, (6), pp. 1191–1197

[11] Chen C., Pana C., Hsieh C., *ET AL.*: 'Liquid-crystal-based terahertz tunable Lyot filter', *Appl. Phys. Lett.*, 2006, **88**, p. 101107

[12] Kaliteevski M., Brand S., Cook J.: 'Terahertz filter based on refractive properties of metallic photonic crystal', *Opt. Express*, 2008, **16**, (10), pp. 7730–7735

[13] MacDonald M., Alexanian A., York R., *ET AL.*: 'Spectral transmittance of lossy printed resonant-grid terahertz bandpass filters', *IEEE Trans. Microw. Theory Tech.*, 2000, **48**, pp. 712–718

[14] Nìmec H., Duvillaret L., Garet F.: 'Thermally tunable filter for terahertz range based on a one-dimensional photonic crystal with a defect', *J. Appl. Phys.*, 2004, **96**, pp. 4072–4075

[15] Chiang Y., Yang C., Yang Y.: 'An ultrabroad terahertz bandpass filter based on multiple-resonance excitation of a composite metamaterial', *Appl. Phys. Lett.*, 2011, **99**, p. 191909

[16] Liang L., Jin B., Wu J.: 'A flexible wideband bandpass terahertz filter using multi-layer metamaterials', *Appl. Phys. B*, 2013, **113**, pp. 285–290

[17] Strikwerda A., Zalkovskij M., Lorenzen D., *ET AL.*: 'Metamaterial composite bandpass filter with an ultra-broadband rejection bandwidth of up to 240 terahertz', *Appl. Phys. Lett.*, 2014, **104**, p. 191103

[18] Kim Y., Lin S., Wu H.: 'A tunable terahertz filter and its switching properties in terahertz region based on a defect mode of a metallic photonic crystal', *J. Appl. Phys.*, 2011, **109**, p. 123111

[19] Vakil A., Engheta N.: 'Transformation optics using graphene', *Science*, 2011, **332**, pp. 1291–1294

[20] Danaeifa M., Granpayeh N., Mohammadi A., *ET AL.*: 'Graphene-based tunable terahertz and infrared band-pass filter', *Appl. Opt.*, 2013, **52**, (22), pp. E68–E72

[21] Sadeghzadeh S., Khatibi M.: 'Effects of physical boundary conditions on the transverse vibration of single-layer graphene sheets', *Appl. Phys. A*, 2016, **122**, (9), pp. 796–807

[22] Sadeghzadeh S., Rezapour N.: 'The mechanical design of graphene nanodiodes and nanotransistors: geometry, temperature and strain effects', *RSC Adv.*, 2016, **6**, pp. 86324–86333

[23] Sadeghzadeh S., Rezapour N.: 'A study of thermal conductivity in graphene diodes and transistors with intrinsic defects and subjected to metal impurities', *Superlattices Microstruct.*, 2016, **100**, pp. 97–111

[24] Manolatou C., Khan M., Fan S., *ET AL.*: 'Coupling of modes analysis of resonant channel add-drop filters', *IEEE J. Quantum Electron.*, 1999, **35**, (9), pp. 1322–1331

[25] Zhu Y., Wang T., Han X., *ET AL.*: 'Plasmon-induced transparency effect in a single circular split-ring core ring resonator side-coupled to a metal-isolator-metal waveguide', *J. Appl. Phys.*, 2015, **117**, (13), p. 133108

[26] Liu H., Ren G., Gao Y., *ET AL.*: 'Tunable subwavelength terahertz plasmon-induced transparency in the InSb slot waveguide side-coupled with two stub resonators', *Appl. Opt.*, 2015, **54**, (13), pp. 3918–3924

[27] Li H., Wang L., Sun B., *ET AL.*: 'Gate-tunable mid-infrared plasmonic planar band-stop filters based on a monolayer graphene', *Plasmonics*, 2016, **11**, (1), pp. 81–93

[28] Garaj S., Hubbard W., Reina A., *ET AL.*: 'Graphene as a sub-nanometer trans-electrode membrane', *Nature*, 2010, **467**, pp. 190–193

[29] Prechtel L., Song L., Schuh D., *ET AL.*: 'Time-resolved ultrafast photocurrents and terahertz generation in freely suspended graphene', *Nat. Commun.*, 2012, **3**, p. 1656